12 | https://doi.org/10.3311/PPci.37602
Creative Commons Attribution

Periodica Polytechnica Civil Engineering, 69(1), pp. 12–27, 2025

3D Printed Concrete: Fresh and Hardened Properties

Marwah M. Thajeel[1*], György L. Balázs[1]

[1] Department of Construction Materials and Technologies, Faculty of Civil Engineering, Budapest University of Technology and Economics, Műegyetem rkp. 3., H-1111 Budapest, Hungary
[*] Corresponding author, e-mail: thajeel.marwah@edu.bme.hu

Received: 04 June 2024, Accepted: 08 August 2024, Published online: 21 August 2024

Abstract

3D concrete printing (3D CP) is an advanced form of additive manufacturing (AM), that allows for the creation of complex geometrical structures using concrete. This technology has the potential to reduce construction time and labour costs while minimizing material waste. However, there are also challenges related to material properties, structural integrity, and standardization of construction practices. The primary challenge in developing 3D printable cementitious materials lies in engineering specific fresh properties that enable extrusion-based printing. Unlike cast concrete, where formwork provides dimensional stability during the printing process, the absence of formwork in 3D printing necessitates fresh mixtures with low-slump and high-thixotropy to be suitable for concrete 3D printing. Additionally, the orthotropic nature of the resulting 3D printed object due to the extrusion process impacts its mechanical properties. Therefore, this research aims to study the effect of water content and loading directions on 3D printed concrete. A pre-mix material from Sika was used in this study. Three mixes were prepared by using three different water to dry material (w/d) ratios, 0.140 l/kg, 0.145 l/kg and 0.150 l/kg. The experiments focused on analysing flowability, green strength, mechanical properties (compressive strength, flexural strength, and modulus of elasticity), water absorption, porosity, and chemical transformations at high temperatures through thermoanalytical measurement. The results showed that the mixture containing 0.145 l/kg (w/d) exhibited satisfactory 3D printability, optimal mechanical performance, lower porosities compared with mixtures 0.140 and 0.150, and same total porosity compared with cast specimen.

Keywords

3D concrete printing, compressive strength, flexural strength, loading directions, modulus of elasticity, water content

1 Introduction

Additive manufacturing (AM), commonly referred to as 3D printing, encompasses a group of innovative methods designed for fabricating three-dimensional objects directly from digital models by depositing successive layers of material, thereby minimizing waste production [1]. The American Society for Testing and Materials (ASTM) defines AM as "the process by which materials are joined to construct objects from 3D model data, typically through a layer-by-layer approach" [2]. 3D concrete printing (3D CP), represents an advanced form of AM. It facilitates the creation of complex geometrical structures, which were challenging to achieve using conventional construction techniques. This innovative approach permits the extrusion of concrete through a nozzle in a sequential layer-by-layer manner, enabling the construction of structural elements without the need for formwork or additional vibration processes [3]. In recent years, a variety of 3D CP methods have been developed to utilize AM in concrete construction industry. Extrusion-based and selective binding (also known as powder-based) techniques are the mainstays of these technologies [4, 5]. This article delves into extrusion-based 3D concrete printing (3DCP). Many companies, like Contour Crafting, CyBe, XtreeE, WinSun, Apis Cor, and more, have been exploring ways to bring this innovative technology to practical use in the real world [6], thereby demonstrating the potential of this technology.

One of the key advantages of 3D CP is its potential to reduce construction time and labour costs while minimizing material waste [7, 8]. Traditional construction methods often involve significant manual labour and are susceptible to errors, leading to delays and cost overruns [9]. In the report of Safe Work Australia [10], 35 construction workers are seriously injured every day in Australia. Furthermore, falls from a height account for more than a quarter of all

Cite this article as: Thajeel, M. M., Balázs, G. L. "3D Printed Concrete: Fresh and Hardened Properties", Periodica Polytechnica Civil Engineering, 69(1), pp. 12–27, 2025. https://doi.org/10.3311/PPci.37602

construction deaths. This is despite the fact that Australia has some of the strictest construction site safety rules in the world. 3D CP, on the other hand, offers the potential for rapid construction of building components, thereby streamlining the overall construction process [11]. Additionally, this technology enables the customization of building components, thereby facilitating the implementation of novel architectural designs and structural solutions [12]. Furthermore, the use of 3D concrete printing has the potential to enhance sustainability in construction by optimizing material usage and reducing carbon emissions associated with traditional construction methods [13].

While 3D concrete printing (3DCP) holds great promise, it also faces several hurdles, particularly concerning material properties, structural integrity, and the standardization of construction practices. One of the biggest challenges in creating 3D printable cement-based materials is engineering them to have the right fresh properties for extrusion-based printing. Unlike traditional cast concrete, which uses formwork to maintain shape during the curing process, 3D printing lacks this support. Therefore, the fresh concrete mixtures need to have low slump and high thixotropy to ensure they are stable and suitable for the 3D printing process [14, 15]. Various studies [4, 8, 16] have investigated the fresh state behaviours of cementitious materials suitable for 3D printing, such as extrudability, open time, and buildability. For instance, Le et al. [8] proposed tests to develop a high-performance fibre-reinforced material for 3D concrete printing, while Kazemian et al. [17] demonstrated ways to assess the printing quality and shape stability of fresh mixtures. Ma et al. [14] used existing tests to find the best mix design for concrete with copper tailings for 3D printing. Moreover, recent advancements have led to new methods for measuring and evaluating the fresh properties of 3D printable cementitious materials [18–22].

Expecting 3D printable cementitious materials to have both good extrudability and buildability might seem contradictory [23]. However, it's crucial to find a balance between the right flowability for extrusion and sufficient strength after deposition [24]. The performance of fresh mixtures under different conditions depends on their rheology and thixotropy. Roussel [25] provided a summary of the necessary rheological properties of cementitious materials for 3D construction printing. Typically, the rheology of concrete is influenced by the mix design, which involves the volume and composition of materials like cement, fillers, and other supplementary components, as well as particle shape, content, aggregate gradation, and the water-to-binder ratio [23, 26]. Additionally, admixtures such as superplasticizers, viscosity modifiers, and accelerators can be used to fine-tune the rheological performance [23].

On the other hand, the other challenge of the 3D CP, lies in the orthotropic nature of the resulting 3D printed object due to the extrusion process. Orthotropy denotes the anisotropic behaviour of a material along different axes resulting from its inherent microstructural characteristics. In the context of 3D printed concrete, the layer-by-layer deposition process introduces variations in material composition and microstructure, thereby impacting its mechanical properties. The study of the orthotropic behaviour of 3D printed concrete enables engineers and researchers to accurately evaluate its strength, stiffness, and durability under diverse loading conditions [27]. Studies conducted on 3D printed concrete involved various tests such as tensile, compression, splitting, and flexural tests [28]. These tests confirmed the evident anisotropic behaviour of 3D printed concrete in comparison to ordinary concrete [29]. Additionally, it was observed that the mechanical properties of 3D printed concrete are influenced by the loading direction, printing direction, and printing parameters [25, 30].

The present study aims to investigate the influence of water content and loading directions on 3D printed concrete. A series of tests have been conducted to explore the effects of water content on the fresh state behaviour of 3D CP, encompassing flowability and green strength. Furthermore, the study delves into the impacts on the mechanical characteristics, including compressive strength, flexural strength, and modulus of elasticity testing at 28 days. Additionally, mechanical tests have been extended to encompass measurements of water absorption, apparent porosity, total porosity, and closed porosity. Moreover, the chemical transformations at high temperatures have been studied through thermoanalythical measurement. Finally, the paper discusses the obtained results.

2 Experimental programme and methods

2.1 Raw material and fresh mixture preparation

To prepare the 3D printed and cast specimens, a pre-mix material called Sikacrete®-751 3D from Sika was used. This material consists of Portland cement, aggregate, and additives. Sikacrete®-751 3D is light grey-white in colour and has an accelerated setting time, making it ideal for better buildability. It features a maximum aggregate size of 1 mm and only requires mixing with water to be ready for use. Fig. 1 gives X-ray diffraction (XRD) patterns of raw

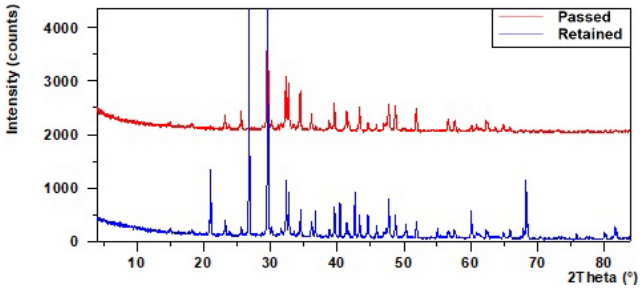

Fig. 1 XRD analysis results of raw pre-mix material

pre-mix material for the passing and retained on sieve size 0.063 mm. XRD was conducted on PANanalytical Xpert Pro MPD powder X-ray diffractometer with X'celerator detector, with Cu-Kα radiation operated at 40 kV and 30 mA, for 2θ values between 3° and 85°.

The water to dry material ratio (w/d) was the main parameter of the different mix designs. Three mixes were prepared by using three different w/d ratios, 0.140 l/kg, 0.145 l/kg and 0.150 l/kg. The fresh mixtures were prepared using a planetary mixer (Hobart) by following the procedures:

1. homogenize the dry components by mixing for 2 min at a low speed,
2. add the water while mixing at a low speed,
3. after 3 min, pause, scrape the walls and blade,
4. mix the mixture again at high speed for 2 min,
5. stop, start the test.

The time zero was defined as the moment when the water was added to the dry mixture.

2.2 Concrete printing process

A mixing pump from MAI (Fig. 2 (b)), was used in this paper. Only the pumping system of this mix was used since the fresh mixtures were prepared by using outside Hobart mixture to make sure adding the exact w/d ratio, additionally to keep the same mixing procedure. After preparing the fresh mixture manually loaded to the feeder system which consist of a hopper (volume: 24 l), and extruder with a barrel and die. A six-axis robot (Fig. 2 (a)) was used for printing process. The robot used for printing can rotate 360 degrees and cover a horizontal diameter of 3 meters and a vertical height of 3 m. With extensions, it can reach up to 6 m. Its printing speed is adjustable, ranging from 0 to 200 mm/s. The robotic arm is connected to a controller that manages its head movements, ensuring precise operation. A flexible hose with an inner diameter of 25 mm and a length of 5 m is used to connect the die to the pump. A nozzle with a circular opening is connected to

(a)

(b)

Fig. 2 3DCP setup; (a) six-axis robot; (b) mixing pump system

the hose and mounted on the robotic print head on the end part of the z-axis. The flow rate, printing speed, and layer height were kept the same for the three mixes as 1.5 l/min, 84 mm/s, and 10 mm, respectively.

In this study, we carefully considered the characteristics of anisotropy. Therefore, it is necessary to establish a coor-

dinate system based on the printing process. We defined the horizontal print plane as the X-Y plane, with the vertical direction across layers as the Z-axis. The X-axis aligned with the direction of the printed layer, following the movement of the nozzle, while the Y-axis was perpendicular to the X direction within the printing plane, where the nozzle moved between layers (Fig. 3).

2.3 Test methods

2.3.1 Flow table test

The test was carried out in accordance with EN 1015-3:1999 [31]. In this test, a mini-cone mould with an upper internal diameter of 70 mm, a bottom internal diameter of 100 mm, and a height of 60 mm was used. Before starting, the inside of the mould was lubricated with mould oil. The mould was half-filled with the fresh mixture, which was then stirred about 10 times with a wooden stick. This process was repeated for the second half of the mould. Any excess material was gently scraped off with a trowel. After removing the mould, the table was dropped 15 times within 15 seconds. The spread diameter was measured in two perpendicular directions. This test was performed for each mixture at 5 minutes, 15 minutes, and 30 minutes, with two repetitions for each time interval.

2.3.2 Green strength test

The green strength test was carried out to evaluate how the strength of the mixtures developed over the first hour. Fresh mixtures were prepared and poured into cylindrical moulds with a 60 mm internal diameter and 60 mm height. While there is no standard for the green strength test, the mould dimensions were chosen based on the available equipment in our laboratory. The moulds were initially coated with silicone spray before filling them with the fresh mortar. To minimize air bubbles, all samples were manually compacted. They were then stored in a sealed plastic bag and demoulded just before testing. The green strength tests were performed using an Instron universal testing machine equipped with a 10 kN load cell, Fig. 4. The test was conducted with constant compression and variable load, as follows:

- Pre-test: speed of 5 mm/min until reaching 4 N.
- Test: speed of 15 mm/min until either a compression of 25 mm or a reduction of the compressive force to 95%, the chosen test limitations were selected based on practical considerations to ensure consistent and reliable testing of the green strength. Since there is no established standard for testing 3D printed concrete, these parameters were determined through preliminary trials to provide stable and repeatable conditions. The pre-test speed allows for a controlled initial application of load, while the test speed is designed to simulate realistic loading conditions and capture the material's response effectively. These settings ensure that the material is neither subjected to excessive deformation too quickly nor allowed to settle for too long, which could affect the accuracy of the results.

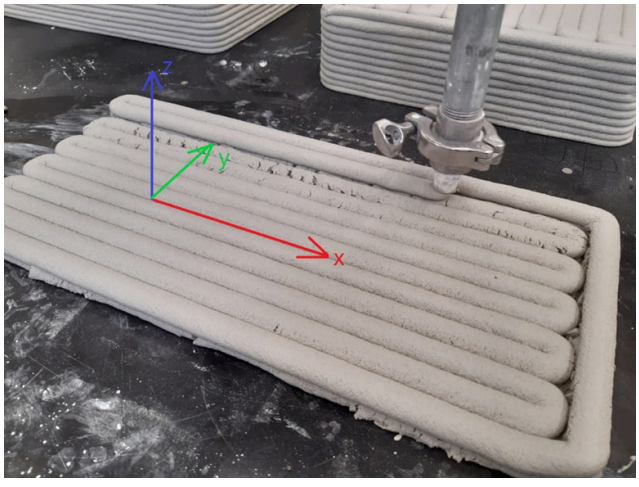

Fig. 3 Coordinate system of the 3D printed specimens (mixture 0.140)

Fig. 4 Green strength test setup

For each mixture, the test was conducted at 5 min, 15 min, 30 min, 45 min and 60 min, with three repetitions for each time interval.

2.3.3 Compressive strength test

A 580 × 286 × 110 mm^3 wall was printed using the printing system described in Section 2.2, (Fig. 5 (a)). The printed samples were cut from the printed wall. To account for the anisotropic mechanical properties of the printed mortar [32], the samples were tested in the X, Y, and Z directions (Fig. 5 (b)), with three repeated tests conducted in each direction. The average value was then calculated from these repeated tests. Thus, for each mixture, nine printed samples were prepared and tested in total. Six cast samples of each mixture were also prepared and tested for comparison purposes. All samples had a dimension of 100 × 100 × 100 mm^3 and were cured in a room temperature. Compressive strength at 28 days was measured conforming EN 12390-3:2019 [33], at a loading rate of 5 kN/s.

2.3.4 Flexural strength test

A 580 × 320 × 90 mm^3 wall was printed (Fig. 6 (a)). Small prisms were cut in two perpendicular directions for the flexural strength test. The printed samples were tested in X, Y, and Z directions (Fig. 6 (b)). The average value was calculated through 3 repeated tests in each direction. Thus, for each mixture, nine printed samples were prepared and tested in total. Six cast samples of each mixture were also prepared and tested. All samples had a dimension of 40 × 40 × 160 mm^3 and were cured in a room temperature. flexural strength at 28 days was measured conforming EN 12390-5:2019 [34], at a loading rate of 0.05 kN/s.

2.3.5 Modulus of elasticity test

A 70 × 70 × 250 mm^3 prisms were cut from the same wall that printed in Section 2.3.4 (Fig. 6 (a)). The printed samples were tested in two directions were the layers horizontal (H) and vertical (V), (Fig. 7 (a)). The average value was calculated through three repeated tests in each direction. Thus, for each mixture, six printed samples were prepared and tested in total. Three cast samples of each mixture were also prepared and tested. The test was performed by EN 12390-13:2013 standard [35]. The surface of the specimen is marked with paint for appropriate contrast, as the strain is measured by a contactless (video) technique (Fig. 7 (b)). The specimen is subjected to a compressive force with maximum third of the compressive strength. The data for stress and strain values were collected, secant

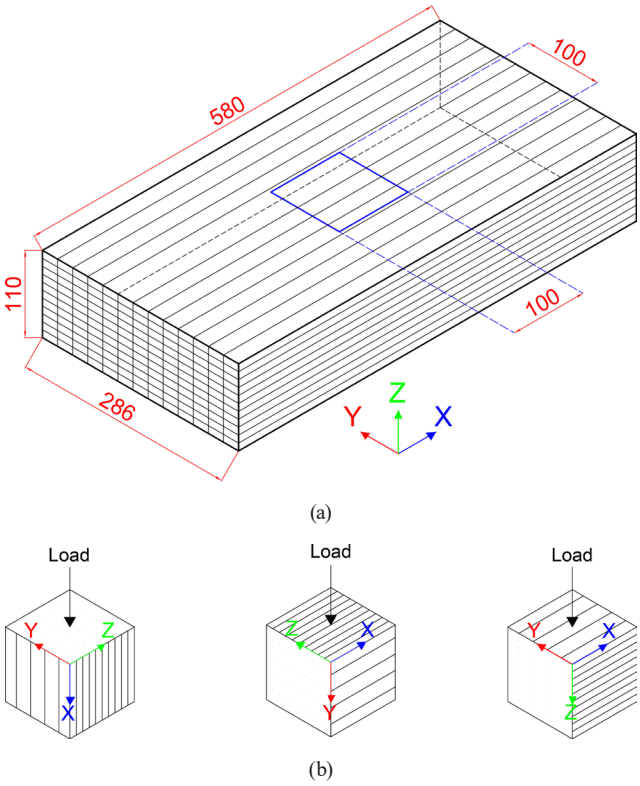

Fig. 5 Schematic diagram illustrating the loading directions for conducting compressive strength tests on printed cubes; (a) 3D printed wall for compressive strength test; (b) Loading directions for 3D printed cubes

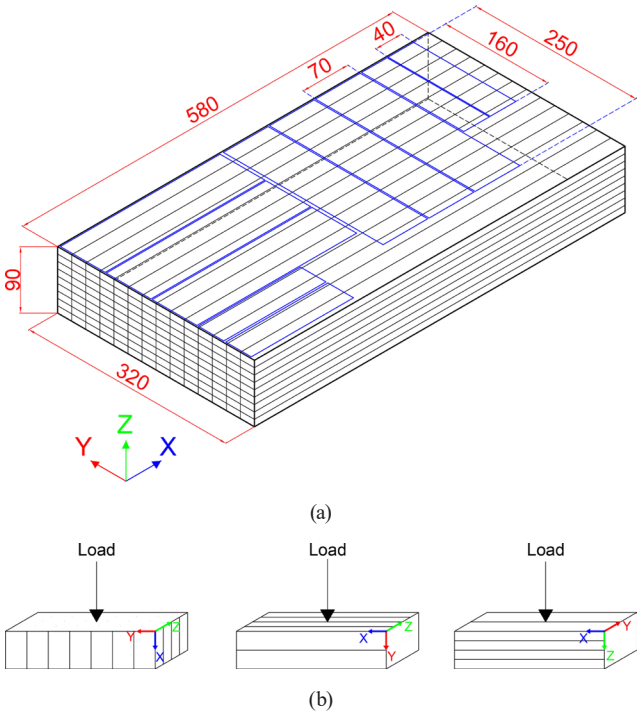

Fig. 6 Schematic diagram illustrating the loading directions for conducting flexural strength tests on printed prisms; (a) 3D printed wall for flexural strength test; (b) Loading directions for 3D printed prisms

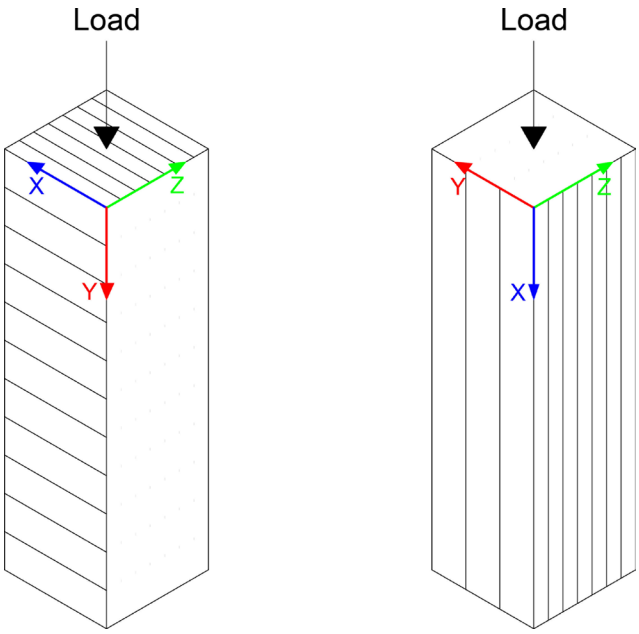

(a)

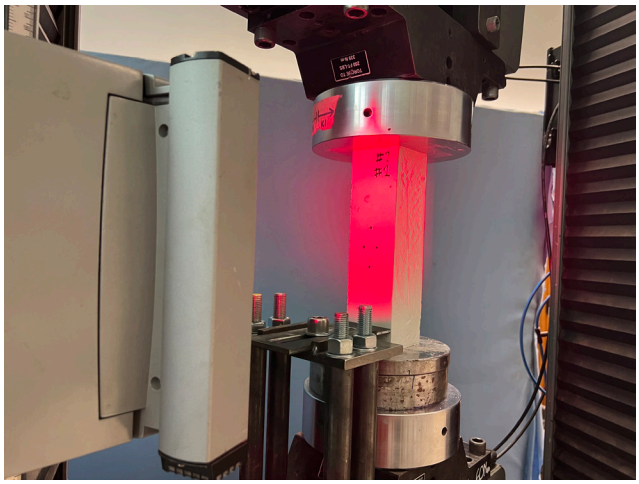

(b)

Fig. 7 Loading directions and test setup for conducting modulus of elasticity test on printed prisms; (a) Loading direction of 3D printed prisms; (b) Test setup

modulus of elasticity was calculated using Eq. (1) from the standard:

$$E_{c,0} = \frac{\Delta\sigma}{\Delta\varepsilon} = \frac{\sigma_a^m - \sigma_b^m}{\varepsilon_{a,1} - \varepsilon_{b,0}}, \tag{1}$$

where $E_{c,0}$ is modulus of elasticity, σ_a^m is upper stress (MPa), σ_b^m is lower stress (MPa), $\varepsilon_{a,1}$ is strain from upper stress (mm/mm), and $\varepsilon_{b,0}$ is strain from lower stress (mm/mm).

2.3.6 Water absorption and porosity tests

Mechanical tests were extended by measurements of water absorption and porosity, which were measured on cube with size 50 × 50 × 50 mm^3 for each mix tested four printed cubes and four cast cubes. For water absorption calculation the specimens were stored in water until constant mass. After saturation the cubes were dried in a drying furnace at 60 °C until constant mass. Therefore, the amount of water uptake could be measured and the volume of open pores could be determined [36]. For the total porosity calculation, the material density was measured by using pycnometer. The dried cubes crushed to powder and measured the material density four times for each mix (printed and cast).

Water absorption refers to the ability of a material to absorb water when immersed in it. It is an important property to assess as excessive water absorption can lead to degradation of the material over time. Apparent porosity is a measure of the volume of open pores in a material relative to its total volume. It is an indicator of the material's ability to absorb water and other liquids. Total porosity, on the other hand, includes both open and closed pores in the material and provides a more comprehensive understanding of its porosity. Closed porosity specifically refers to the volume of pores that are not interconnected and are therefore not accessible to external fluids. The water absorption, open porosity total porosity, and close porosity were calculated by using Eqs. (2) to (5):

$$\text{Water absorption: } w(m\%) = \frac{m_{\text{wet}} - m_{\text{dry}}}{m_{\text{dry}}} \times 100, \tag{2}$$

$$\text{Apparent porosity: } p_a = w(m\%) \times (\text{dry density}/\text{water density}), \tag{3}$$

$$\text{Total porosity} = 1 - (\text{dry density}/\text{material density}), \tag{4}$$

$$\text{Close porosity} = \text{total porosity} - \text{apparent porosity}, \tag{5}$$

where m_{wet} is the saturated mass and m_{dry} is the dried mass.

To support the porosity results scanning electron microscope investigations were conducted (SEM), for cast (C) and printed specimens. The 50 mm cubes were crushed, and the tested samples have been taken from the core of the cross-sectional areas of the specimen, then the samples faces were coated with golden spray for 30 s in a vacuum chamber and thereafter, the samples are investigated under SEM.

2.3.7 Thermoanalythical test

The chemical changes in the selected mixtures as they were exposed to increasing temperatures were examined using a MOM Q-1500 D derivatograph. In this test, the powdered material was heated up to 1000 °C, while the

device recorded thermogravimetric (TG), derivative thermogravimetric (DTG), and differential thermoanalytical (DTA) data [37]. Thermoanalythical tests were made at the age of 28 days and the test parameters were:

- Reference substance: aluminum oxide;
- Heating rate: 10 °C/min;
- Temperature range: 20–1000 °C;
- TG sensitivity: 500 mg;
- Crucible: corundum;
- Atmospheric pressure.

3 Results and discussion

3.1 Flowability

Fig. 8 shows the results of the flow test results of mixtures with three w/d ratios at different ages. The spread diameter of all mixtures gradually decreases over time, indicating that the workability of the fresh mixtures diminishes as resting time increases. This reduction in workability is likely due to the gradual stiffening of the mixture. This stiffening occurs because calcium silicate hydrate (C-S-H) bridges form between particles, creating a rigid, interconnected network within the material [38]. Mixture 0.140 showed lower flowability at any specific age compared with mixtures 0.145 and 0.150. Thus, may lead an issue to pump and extrude concrete with low fluidity. While mixture 0.150 demonstrated the highest fluidity after mixing by about 7% and 17% as compared with mixtures 0.145 and 0.140, respectively. However, it's noteworthy that the decrease in flowability with age is more pronounced for mixture 0.150. For instance, the flowability decreases by 20% after 30 min as compared with other mixtures. Mixture 0.145 seems to provide a good balance between flowability and stability, as it offers relatively good initial flowability (144.5 mm) and maintains reasonable flowability after 30 minutes (120.8 mm).

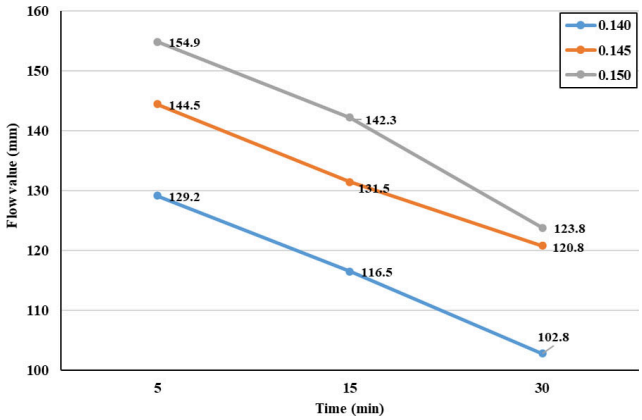

Fig. 8 Flowability test results of mixtures with different w/d ratios at different ages

Moreover, during printing the three mixtures by using the printing system described in Section 2.2, the extrusion pressure was recorded. It is obvious that the mixture containing a lower w/d ratio requires higher extrusion pressure to reach a similar material flow rate compared to mixture containing higher w/d ratios. The extrusion pressure for the mixture 0.140 was ranging from 18–20 bar. While for the mixtures 0.145 and 0.150 were ranging from 12–15 bar and from 6–10 bars respectively.

3.2 Green strength results

The green strength development within the first hour could be used as an indicator of the proper structural buildability of the mixture. Fig. 9 (a)–(c) shows the average load-displacement curves of the mixtures 0.140, 0.145, and 0.150 from the age 5 min to 60 min. while Fig. 9 (d) shows the green strength of each test defined as the peak load divided by the surface area of the cylinder. The green strength of the mixtures 0.145 and 0.150 were close at younger ages 5 min – 15 min and lower than mixture 0.140. After that, the mixture 0.145 tends to be close to the mixture 0.140 and much higher than the mixture 0.150. Indicating that this ratio may be optimal for achieving good early strength with low pressure for pumpability requirement and great strength development for buildability purpose in 3D printed concrete.

3.3 Compressive strength results

Fig. 10 demonstrates the results referring to the compressive strength of the casted and printed cubes of the three mixtures after 28 days. The results showed that the compressive strength of the cast cubes (C), is greater than the compressive strength of the printed cubes. Similar results have also been reported in previous studies [39–41]. This mechanical variation in printed samples may be due to the inadequate interface strength and printing precision [39]. In particular, the anisotropy in the compressive strength of the printed cubes was observed, depending on the loading direction. Importantly, the X direction is parallel to the printing direction, which generally indicates higher particle placement and compaction compared to the Y and Z directions. This is evident in the results for the mixtures with w/d ratios of 0.145 and 0.150, where the X direction shows superior performance in terms of compressive strength. For the stiff mixture with a w/d ratio of 0.140, however, the highest compressive strength was observed in the Y direction. This deviation could be due to the specific characteristics of the stiffer mixture, such as its reduced workability, leading to variations in layer bonding and compaction across different directions. Furthermore,

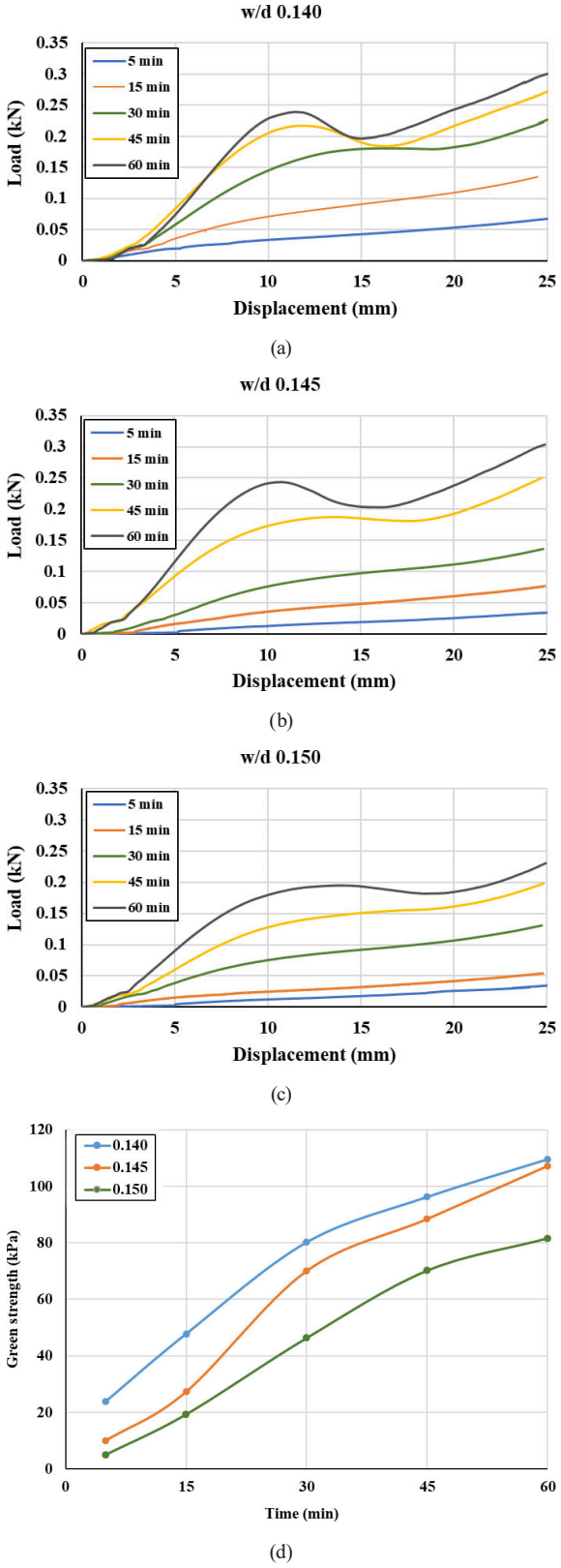

Fig. 9 Load-displacement curve and green strength of fresh mixtures; (a) Load-displacement curve of mixture 0.140; (b) Load-displacement curve of mixture 0.145; (c) Load-displacement curve of mixture 0.150; (d) Green strength of the three mixtures

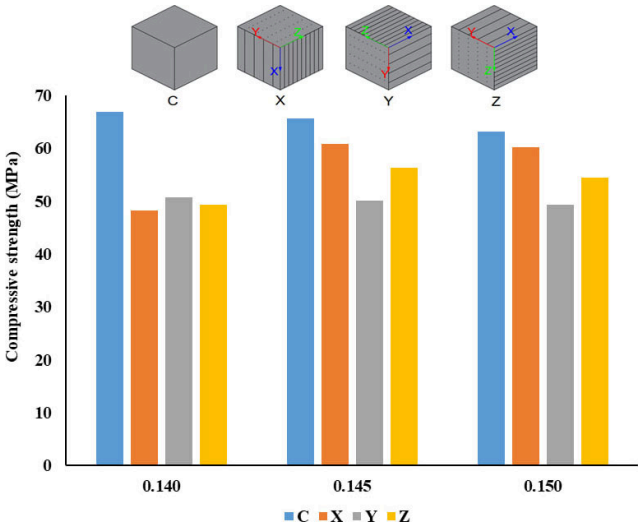

Fig. 10 Compressive strength test results at 28 days

Nerella et al. [27] commented that the compaction induced by the layer weight should also be considered when assessing the variation of the compressive strength.

In general, the compressive strength of concrete tends to decrease as the water-to-dry material (w/d) ratio increases, similar to conventional concrete where too much water weakens the structure. However, for 3D printing concrete, the compressive strength tends to increase with a higher w/d ratio. The mixture with a 0.140 w/d ratio had the lowest compressive strength for printed cubes but the highest for cast ones. This mixture was too stiff, causing many cracks in the extruded layers, which negatively affected its overall mechanical properties (see Fig. 11 (a)). The lower water content altered the anisotropic behaviour of the printed cubes, with the Y loading direction showing about 5% and 3% higher compressive strength than the X and Z directions, respectively.

The 0.145 mixture showed the best compressive strength at 28 days in all three loading directions compared to the 0.150 and 0.140 mixtures (see Fig. 11 (b)). The average compressive strength in the X direction was about 17% higher than in the Y direction and 7% higher than in the Z direction. Meanwhile, the 0.150 mixture had results similar to the 0.145 mixture, with the average compressive strength in the X direction being about 19% higher than in the Y direction and 10% higher than in the Z direction.

3.4 Flexural strength results

Previous research on mechanical properties has demonstrated that 3D printing using cementitious materials results in noticeable anisotropy behaviour once the material hardens [42, 43]. Fig. 12 shows the flexural strength

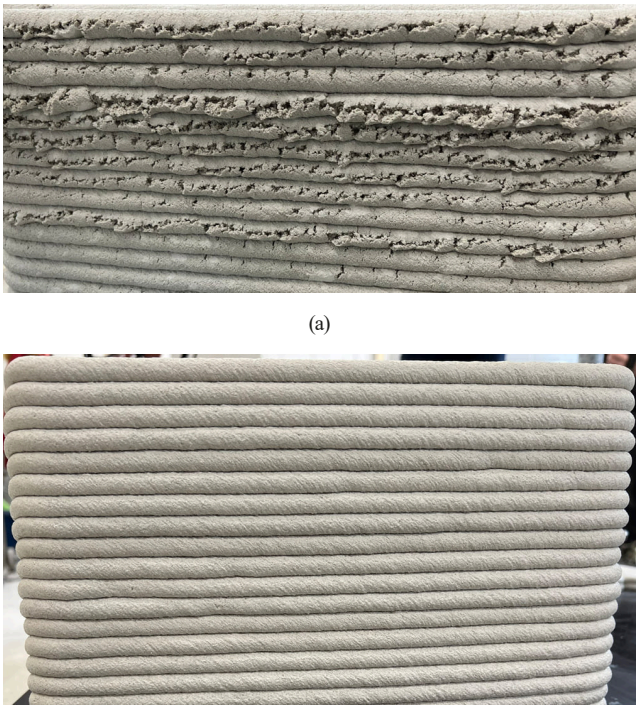

(a)

(b)

Fig. 11 Quality of the printed walls; (a) w/d = 0.140; (b) w/d = 0.145

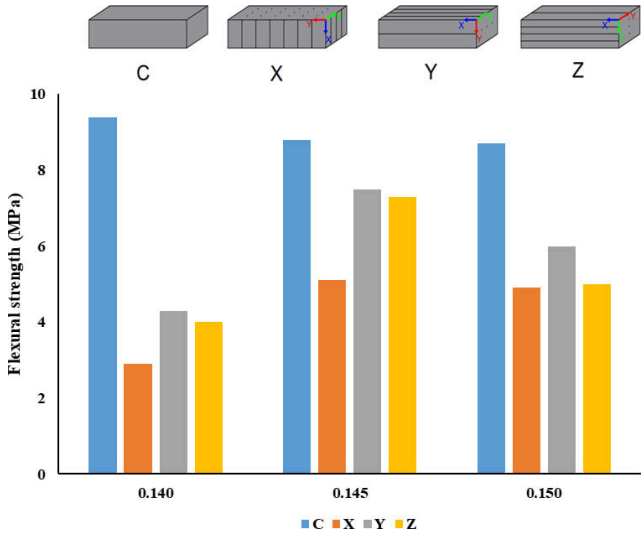

Fig. 12 Flexural strength test results at 28 days

test results in this study. It's observed that using the 0.145 w/d ratio tends to enhance the flexural strength of the printed specimens. However, they still exhibit significant anisotropy, which differs notably from traditionally cast specimens. This characteristic can be seen as inherent property to 3D printed layered structures.

When subjected to loading in the X, Y, and Z directions, the flexural strength is highest in the Y and Z directions, showing similar performance, while the flexural strength in the X direction is relatively lower. With 0.145 l/kg water to dry material ratio, 3D printed prisms loaded in Y and Z directions showed the highest flexural strength 7.5 MPa and 7.3 MPa, respectively. While the flexural strength of the specimens when loaded in X direction were 5.1 MPa. The flexural strength of the cast specimens was 8.8 MPa and higher than that of printed specimens tested in X, Y, and Z directions by about 42%, 15%, and 17%, respectively. Same anisotropic behaviour was showed in the other mixtures. Mixture 0.150 showed close results to mixture 0.145, the flexural strength of the cast specimens and printed specimens loaded in X, Y, and Z directions were 8.7 MPa, 4.9 MPa, 6 MPa, and 5 MPa, respectively. Meanwhile, the mixture 0.140 showed the highest flexural strength of the cast specimens 9.4 MPa and the lowest flexural strength of printed specimens tested in X, Y, and Z directions 2.9 MPa, 4.3 MPa, and 4 MP, respectively. This can be explained due to the extruded concrete in this mixture was too stiff and the outer parts of the layers sheared off and the bonding between the excessive layers were weak and that effect negatively on the overall mechanical characteristics.

The primary cause of the pronounced anisotropy in 3D printed specimens is the layered structure formed during the printing process. Within this structure, voids and weak contact interfaces typically develop between adjacent layers aligned with the printing direction. These imperfections significantly influence the bending performance of the specimen when subjected to different loading directions. During bending, the specimen's ultimate strength is typically dictated by the maximum normal stress at its midpoint. When loaded in the X direction, the tensile stress at the midpoint runs perpendicular to the layer-to-layer interface of the specimen, where the bond strength is weakest.

3.5 Modulus of elasticity results

The modulus of elasticity results of the cast specimens (C), and printed specimens tested in two directions when the layers vertical (V, parallel to the loading direction), and horizontal (H, perpendicular to the loading direction), were shown in Fig. 13.

The results showed a higher modulus of elasticity for cast specimen compared with printed specimens. With increasing w/d ratio from 0.140 l/kg to 0.150 l/kg, a slight reduction of the modulus of elasticity for cast specimens was observed from 34 GPa to 30 GPa. Meanwhile, for 3D printed specimens, the modulus of elasticity was found to be significantly influenced by the water content and loading directions. All mixtures showed the same anisotropic behaviour, a higher modulus of elasticity was found when

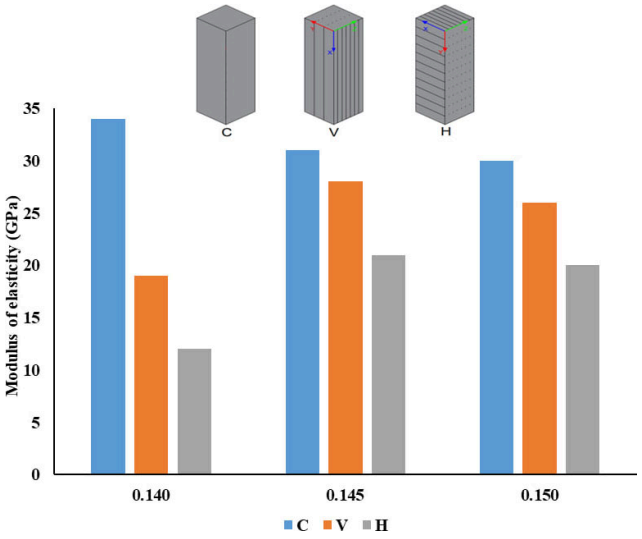

Fig. 13 Modulus of elasticity test results at 28 days

the loading directions parallel to the printing directions (V) compared to when the loading directions perpendicular to the printing directions (H). During the 3D printing process, layers are deposited sequentially, creating a structure with distinct directional properties. When the load is applied parallel to the printing direction, the stress is distributed along the continuous filaments of the printed layers, which enhances the material's stiffness and results in a higher modulus of elasticity. In contrast, when the load is applied perpendicular to the printing direction, the stress must traverse the interfaces between layers, which are typically weaker due to the presence of micro-gaps, lower bonding strength, and potential defects. This interlayer weakness leads to lower stiffness and, consequently, a lower modulus of elasticity. This behaviour is a common characteristic of additively manufactured materials and reflects the directional dependency of their mechanical properties.

The 0.140 mixture showed the lowest modulus of elasticity 19 GPa and 12 GPa in V and H directions, respectively. Mixtures 0.145 and 0.150 showed close results 28 GPa, 21 GPa, 26 GPa, and 20 GPa in V and H directions, respectively.

3.6 Microstructure results

Fig. 14 presents the variations in body and material densities between conventionally cast cubes and those fabricated through 3D printing techniques. A comparative analysis reveals that the average hardened density of 3D printed cubes marginally exceeds that of their cast counterparts. This increase in density for 3D printed cubes, corroborated by findings in literature [41, 44], can be attributed to the enhanced compaction achieved under the extrusion

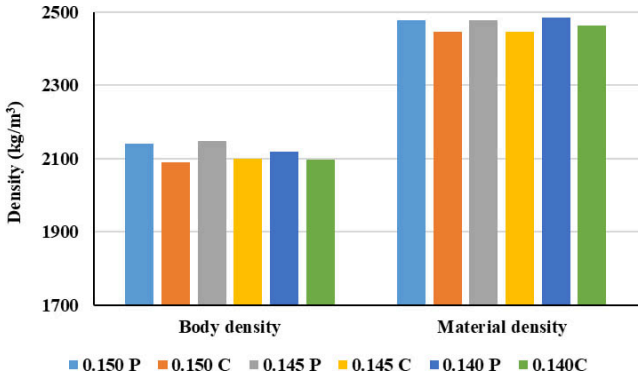

Fig. 14 Body and material densities of cast (C) and printed (P) specimens

process's pressure. Additionally, the selection of samples from the central portion of the printed wall, which is subject to greater compaction relative to outer layers, further contributes to this observed density increment.

Fig. 15 delineates the water absorption rates, along with apparent, total, and closed porosity values for both cast and 3D printed specimens. It is evident that the water absorption rates for 3D printed cubes were higher than those of the cast cubes by approximately 33%, 14%, and 43% for mixtures 0.150, 0.145, and 0.140, respectively. Notably, the mixture with w/d ratio 0.145 exhibited the lowest water absorption rate among the tested specimens, indicating a reduction of approximately 35% and 37% for 3D printed cubes, and 5% and 10% for cast cubes, in comparison with mixtures 0.150 and 0.140, respectively.

Furthermore, the study found that the apparent porosity (open porosity) in 3D printed cubes was significantly higher than in cast cubes, with variations of about 32%, 15%, and 42% for the respective mixtures. Conversely, the total porosity for printed cubes exceeded that of cast cubes by approximately 10% and 11% for mixtures 0.150 and 0.140, respectively, while the values for mixture 0.145

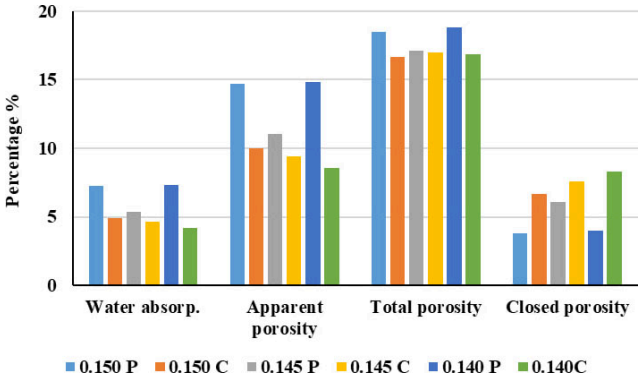

Fig. 15 Water absorption, apparent porosity, total porosity and closed porosity for cast (C) and printed (P) specimens

remained comparable between both types. Interestingly, the closed porosity observed in printed cubes was markedly lower than in cast cubes for all mixtures, showcasing reductions of about 75%, 25%, and 109%, respectively.

These results are supported by the scanning electron microscope (SEM). As shown in Fig. 16, the stiff and wet mixes 0.140 and 0.150, respectively showed more voids than the mixture with w/d ratio 0.145.

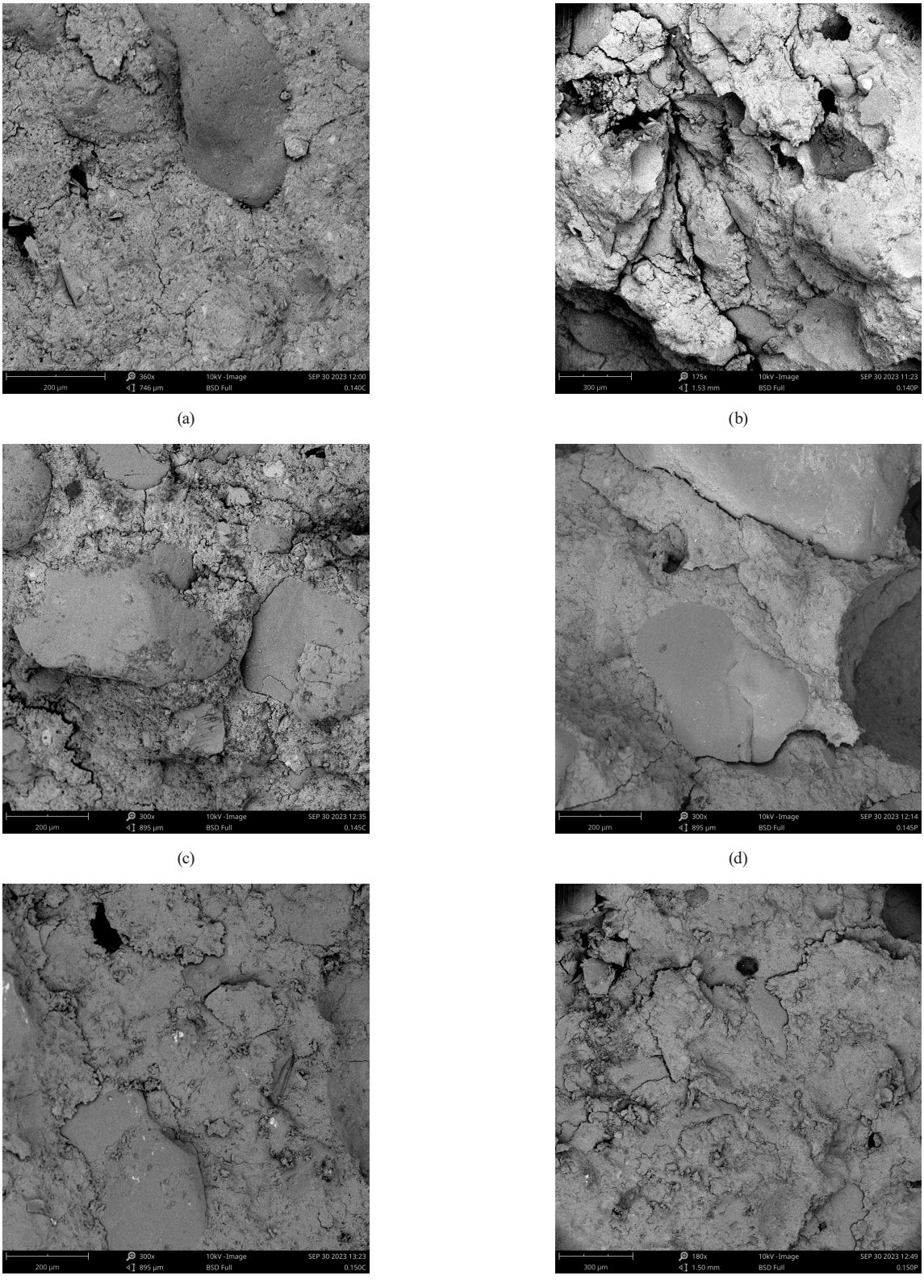

(a) (b) (c) (d) (e) (f)

Fig. 16 SEM images for cast (C) and printed (P) specimens; (a) 0.140 C; (b) 0.140 P; (c) 0.145 C; (d) 0.145 P; (e) 0.150 C; (f) 0.150 P

These observations underscore the distinct porosity characteristics of 3D printed concrete, predominantly open porosity, in contrast to the predominantly closed porosity observed in cast concrete. This distinction likely stems from the layer-by-layer extrusion process inherent to 3D printing. Moreover, the process of printing with either stiff or wet concrete mixtures introduces a more extensive void system within the 3D printed elements, particularly at the interlayer junctions, thereby exerting a substantial influence on the mechanical properties of the material.

3.7 Thermoanalythical results

Thermoanalythical tests were made at the age of 28 days. The results of the thermoanalythical test (Fig. 17) show

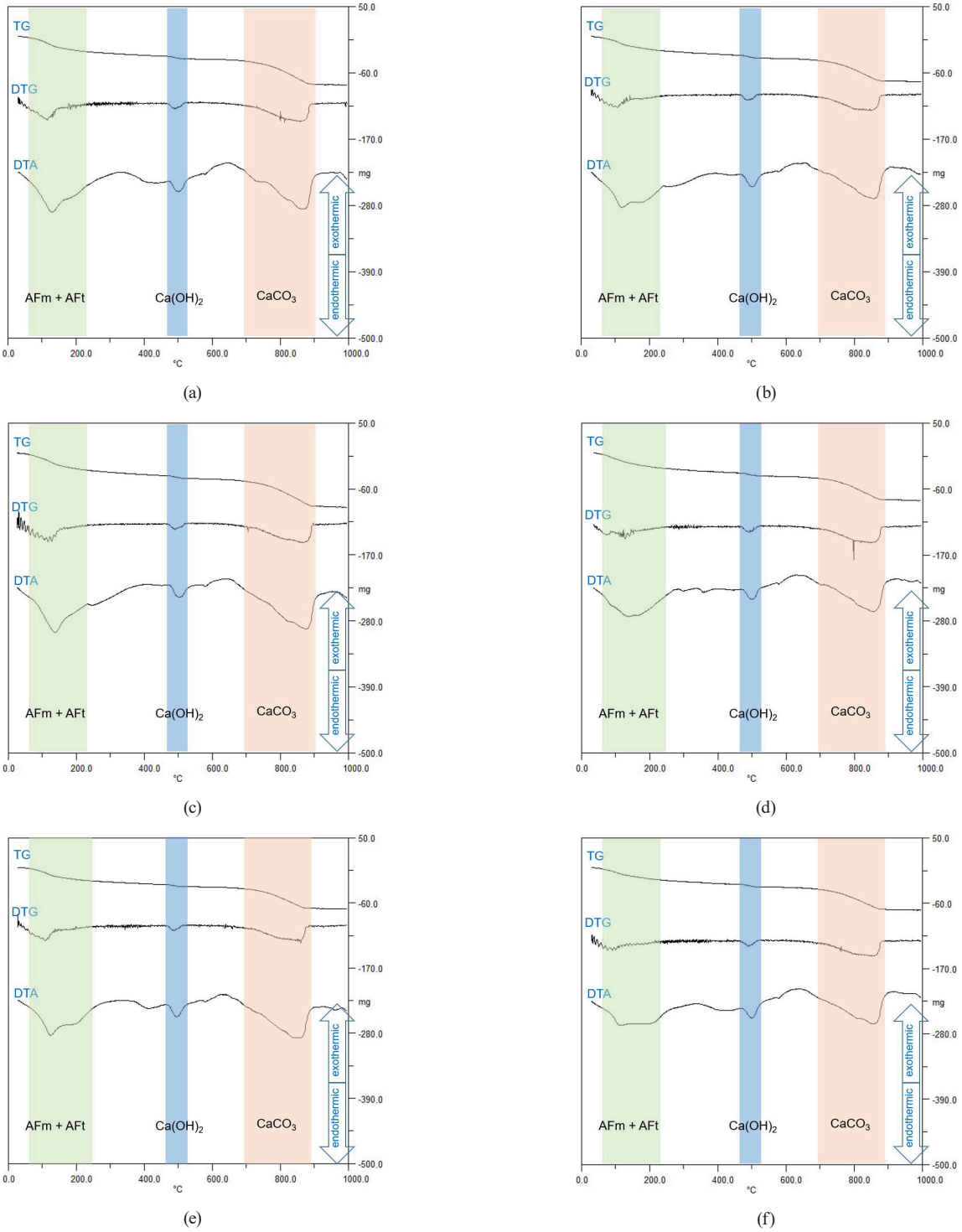

Fig. 17 TG/DTG/DTA curves for cast (C) and printed (P) specimens; (a) 0.150 C; (b) 0.150 P; (c) 0.145 C; (d) 0.145 P; (e) 0.140 C; (f) 0.140 P

that for all mixtures, three mean peaks appear on the DTG and DTA curves. Two series of calcium aluminates, AFm (mono-substituted) and AFt (tri-substituted), appear, with the first main peak occurring at a temperature interval of about 50 °C to 200 °C; on the second peak appears at the temperature around 500 °C, represents calcium hydroxide $Ca(OH)_2$ one hydration product of cement. Meanwhile, the derivative thermogravimetry (DTG) peak between 700 °C to 900 °C indicates the presence of calcium carbonate $CaCO_3$. $CaCO_3$ can be either the reaction product of the $Ca(OH)_2$ and airborne CO_2, or present in the original pre-mix.

Fig. 18 shows the three mean peaks as a mass loss as well as shows the loss of ignition (LOI) which represents the total TG mass deficit during heating up to 1000 °C (m/m%).

Based on the thermoanalythical test results, we can conclude, that the higher total amount of AFm and Aft phases were formed in the mixtures of 0.145 (both cast and printed), which can help in the setting and achieve the stability. Also, the LOI was the higher for specimens of 0.145, which shows the optimum w/d ratio (Fig. 18).

4 Conclusions

An extensive experimental study was carried out on fresh and hardened properties of 3D printed concretes including flowability, green strength, compressive strength, flexural strength, modulus of elasticity, water absorption, porosity, and chemical transformations at high temperatures through derivatographic measurements. Test parameters were the amount of mixing water and testing direction. A pre-mix material from Sika was used in this study. Three mixes were prepared by using three different water to dry material (w/d) ratios, 0.140 l/kg, 0.145 l/kg and 0.150 l/kg. The following conclusions could be obtained in this study:

1. Flowability
   Increasing w/d ratio from 0.140 to 0.150 could increase the flowability and reduce the extrusion pressure and green strength. Mixture 0.145 seems to provide a good balance between *flowability* and stability, as it offers relatively good initial flowability (144.5 mm) and maintains reasonable flowability after 30 minutes (120.8 mm), which provide longer open time. Good early strength with low pressure for pumpability requirement and great strength development for buildability purpose.
2. Compressive strength
   Anisotropy of the printed specimens appears to be critical concerning compressive strength tests. For mixtures 0.145, and 0.150, printed samples were stronger in the loading direction X in comparison with directions Y and Z. The X direction is parallel to the printing direction; this indicates higher particle placement and compaction compared to the Y and Z directions. Mixture 0.145 showed the highest *compressive strength* at 28 days by about 60.9 MPa at X direction. Meanwhile, the 0.140 mixture showed the lowest compressive strength for printed cubes by about 48.3 MPa in X direction. The mixture was too stiff and lots of cracks happened to the extruded layers and that effect negatively on over all the mechanical characteristics.
3. Flexural strength
   Increasing the w/d ratio tends to enhance the *flexural strength* of the printed specimens. However, they still exhibit significant anisotropy, which differs notably from traditionally cast specimens. This characteristic can be seen as inherent property to 3D printed layered structures. The flexural strength is highest in the Y and Z directions, showing similar performance, while the flexural strength in the X direction is relatively lower. With 0.145 l/kg water to dry material ratio, the flexural strength of the cast specimens was higher than that of printed specimens tested in X, Y, and Z directions by about 42%, 15%, and 17%, respectively.
4. Modulus of elasticity
   A higher modulus of elasticity was observed in cast specimens compared to printed specimens. With increasing w/d ratio from 0.140 l/kg to 0.150 l/kg, a slight reduction of the modulus of elasticity for cast specimens was observed from 34 GPa to 30 GPa. Meanwhile, for 3D printed specimens, the modulus of elasticity was found to be significantly influenced by the water content and loading directions. All mixtures showed the same anisotropic

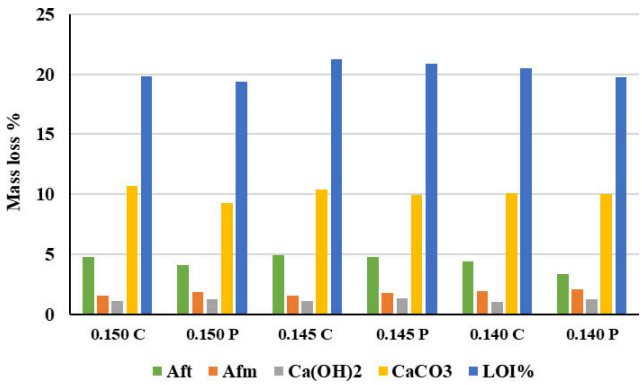

Fig. 18 Mass loss and LOI of the cast (C) and printed (P) specimens

behaviour, a higher modulus of elasticity was found when the loading directions parallel to the printing directions (V) compared to when the loading directions perpendicular to the printing directions (H). The 0.140 mixture showed the lowest modulus of elasticity 19 GPa and 12 GPa in V and H directions, respectively. Mixtures 0.145 and 0.150 showed close results 28 GPa, 21 GPa, 26 GPa, and 20 GPa in V and H directions, respectively.

5. Water absorption and porosity
   Water absorption, apparent porosity (open porosity), total porosity for printed specimens were higher than that for cast specimens. However, the closed porosity was the lower, this indicates the porosity type in the printed specimens is open porosity, while in the cast specimens is closed one. Mixture 0.145 showed the lowest water absorption, apparent, total and closed porosities compared with the mixtures 0.140 and 0.150. Although, it has a higher apparent porosity and lower closed porosity, however the total porosity was the same as compared to the cast specimens.
6. Thermoanalythical test results
   Based on the *thermoanalythical test results*, we can conclude, that the higher total amount of AFm and Aft phases were formed in the mixtures of 0.145 (both cast and printed), which can help in the setting and achieve the stability. Also, the LOI was the higher for specimens of 0.145, which shows the optimum w/d ratio.

Acknowledgements

The *Stipendium Hungaricum Scholarship* Program is highly acknowledged for supporting the PhD study and research work. Authors acknowledge the support by the Hungarian Research Grant VKE 2018-1-3-1_0003 "Development of advanced concrete elements". Thanks to Balázs Burai, Ameen H. Chalawi, as well as Dr. Sándor Sólyom for their help in the printing process and the laboratory measurements. Special thanks to Dr. Katalin Kopecskó for her help in evaluating derivatographic measurements and reviewing the paper, as well as thanks to Prof. Éva Lublóy for her help in reviewing the paper.

References

[1] Nematollahi, B., Xia, M., Sanjayan, J. "Current Progress of 3D Concrete Printing Technologies", In: 2017 Proceedings of the 34th International Symposium on Automation and Robotics in Construction (ISARC), Taipei, Taiwan, 2017, pp. 260–267. ISBN 978-80-263-1371-7
https://doi.org/10.22260/ISARC2017/0035

[2] ASTM "ASTM F2792-10 Standard Terminology for Additive Manufacturing Technologies", ASTM International, West Conshohocken, PA, USA, 2010.
https://doi.org/10.1520/F2792-10

[3] Paolini, A., Kollmannsberger, S., Rank, E. "Additive manufacturing in construction: A review on processes, applications, and digital planning methods", Additive Manufactiring, 30, 100894, 2019.
https://doi.org/10.1016/j.addma.2019.100894

[4] Nerella, V., N., Näther, M., Iqbal, A., Butler, M., Mechtcherine, V. "Inline quantification of extrudability of cementitious materials for digital construction", Cement and Concrete Composites, 95, pp. 260–270, 2019.
https://doi.org/10.1016/j.cemconcomp.2018.09.015

[5] Chen, Y., Veer, F., Çopuroğlu, O. "A critical review of 3D concrete printing as a low CO_2 concrete approach", Heron, 62(3), pp. 167–194, 2017.

[6] Chaves Figueiredo, S., Romero Rodríguez, C., Ahmed, Z. Y., Bos, D. H., Xu, Y., Salet, T. M., Çopuroğlu, O., Schlangen, E., Bos, F. P. "An approach to develop printable strain hardening cementitious composites", Materials & Design, 169, 107651, 2019.
https://doi.org/10.1016/j.matdes.2019.107651

[7] Al Rashid, A., Khan, S. A., G. Al-Ghamdi, S., Koç, M. "Additive manufacturing: Technology, applications, markets, and opportunities for the built environment", Automation in Construction, 118, 103268, 2020.
https://doi.org/10.1016/j.autcon.2020.103268

[8] Le, T. T., Austin, S. A., Lim, S., Buswell, R. A., Gibb, A. G. F., Thorpe, T. "Mix design and fresh properties for high-performance printing concrete", Materials and Structures, 45(8), pp. 1221–1232, 2012.
https://doi.org/10.1617/s11527-012-9828-z

[9] De Schutter, G., Lesage, K., Mechtcherine, V., Nerella, V. N., Habert, G., Agusti-Juan, I. "Vision of 3D printing with concrete – Technical, economic and environmental potentials", Cement and Concrete Research, 112, pp. 25–36, 2018.
https://doi.org/10.1016/j.cemconres.2018.06.001

[10] Australia, S. W. "Work-related injuries and fatalities in construction", [online] Available at: https://www.abs.gov.au/ [Accessed: 20 October 2023]

[11] Arunothayan, A. R., Nematollahi, B., Ranade, R., Bong, S. H., Sanjayan, J. G., Khayat, K. H. "Fiber orientation effects on ultra-high performance concrete formed by 3D printing", Cement and Concrete Research, 143, 106384, 2021.
https://doi.org/10.1016/j.cemconres.2021.106384

[12] Lloret, E., Shahab, A. R., Linus, M., Flatt, R. J., Gramazio, F., Kohler, M., Langenberg, S. "Complex concrete structures: Merging existing casting techniques with digital fabrication", Computer-Aided Design, 60, pp. 40–49, 2015.
https://doi.org/10.1016/j.cad.2014.02.011

[13] Nematollahi, B., Sanjayan, J., Shaikh, F. U. A. "Synthesis of heat and ambient cured one-part geopolymer mixes with different grades of sodium silicate", Ceramics International, 41(4), pp. 5696–5704, 2015. https://doi.org/10.1016/j.ceramint.2014.12.154

[14] Ma, G., Li, Z., Wang, L. "Printable properties of cementitious material containing copper tailings for extrusion based 3D printing", Construction and Building Materials, 162, pp. 613–627, 2018. https://doi.org/10.1016/j.conbuildmat.2017.12.051

[15] Lim, S., Buswell, R. A., Le, T. T., Austin, S. A., Gibb, A. G. F., Thorpe, T. "Developments in construction-scale additive manufacturing processes", Automation in Construction, 21, pp. 262–268, 2012. https://doi.org/10.1016/j.autcon.2011.06.010

[16] Wangler, T., Roussel, N., Bos, F. P., Salet, T. A. M., Flatt, R. J. "Digital Concrete: A Review", Cement and Concrete Research, 123, 105780, 2019. https://doi.org/10.1016/j.cemconres.2019.105780

[17] Kazemian, A., Yuan, X., Cochran, E., Khoshnevis, B. "Cementitious materials for construction-scale 3D printing: Laboratory testing of fresh printing mixture", Construction and Building Materials, 145, pp. 639–647, 2017. https://doi.org/10.1016/j.conbuildmat.2017.04.015

[18] Wolfs, R. J. M., Bos, F. P., Salet, T. A. M. "Early age mechanical behaviour of 3D printed concrete: Numerical modelling and experimental testing", Cement and Concrete Research, 106, pp. 103–116, 2018. https://doi.org/10.1016/j.cemconres.2018.02.001

[19] Reiter, L., Wangler, T., Roussel, N., Flatt, R. J. "The role of early age structural build-up in digital fabrication with concrete", Cement and Concrete Research, 112, pp. 86–95, 2018. https://doi.org/10.1016/j.cemconres.2018.05.011

[20] Wolfs, R. J. M., Bos, F. P., Salet, T. A. M. "Triaxial compression testing on early age concrete for numerical analysis of 3D concrete printing", Cement and Concrete Composites, 104, 103344, 2019. https://doi.org/10.1016/j.cemconcomp.2019.103344

[21] Alghamdi, H., Nair, S. A. O., Neithalath, N. "Insights into material design, extrusion rheology, and properties of 3D-printable alkali-activated fly ash-based binders", Materials & Design, 167, 107634, 2019. https://doi.org/10.1016/j.matdes.2019.107634

[22] Rahul, A. V., Santhanam, M., Meena, H., Ghani, Z. "3D printable concrete: Mixture design and test methods", Cement and Concrete Composites, 97, pp. 13–23, 2019. https://doi.org/10.1016/j.cemconcomp.2018.12.014

[23] Marchon, D., Kawashima, S., Bessaies-Bey, H., Mantellato, S., Ng, S. "Hydration and rheology control of concrete for digital fabrication: Potential admixtures and cement chemistry", Cement and Concrete Research, 112, pp. 96–110, 2018. https://doi.org/10.1016/j.cemconres.2018.05.014

[24] Perrot, A., Rangeard, D., Pierre, A. "Structural built-up of cement-based materials used for 3D-printing extrusion techniques", Materials and Structures, 49(4), pp. 1213–1220, 2016. https://doi.org/10.1617/s11527-015-0571-0

[25] Roussel, N. "Rheological requirements for printable concretes", Cement and Concrete Research, 112, pp. 76–85, 2018. https://doi.org/10.1016/j.cemconres.2018.04.005

[26] Chen, Y., Veer, F., Copuroglu, O., Schlangen, E. "Feasibility of Using Low CO_2 Concrete Alternatives in Extrusion-Based 3D Concrete Printing", In: First RILEM International Conference on Concrete and Digital Fabrication – Digital Concrete 2018, Zurich, Switzerland, 2018, pp. 269–276. ISBN 978-3-319-99518-2 https://doi.org/10.1007/978-3-319-99519-9_25

[27] Nerella, V. N., Hempel, S., Mechtcherine, V. "Effects of layer-interface properties on mechanical performance of concrete elements produced by extrusion-based 3D-printing", Construction and Building Materials, 205, pp. 586–601, 2019. https://doi.org/10.1016/j.conbuildmat.2019.01.235

[28] Yu, K., McGee, W., Ng, T. Y., Zhu, H., Li, V. C. "3D-printable engineered cementitious composites (3DP-ECC): Fresh and hardened properties", Cement and Concrete Research, 143, 106388, 2021. https://doi.org/10.1016/j.cemconres.2021.106388

[29] Pasco, J., Z. Lei, Z., Aranas Jr., C. "Additive Manufacturing in Off-Site Construction: Review and Future Directions", Buildings, 12(1), 53, 2022. https://doi.org/10.3390/buildings12010053

[30] Roussel, N., Spangenberg, J., Wallevik, J., Wolfs, R. "Numerical simulations of concrete processing: From standard formative casting to additive manufacturing", Cement and Concrete Research, 135, 106075, 2020. https://doi.org/10.1016/j.cemconres.2020.106075

[31] European Committee for Standardization "EN 1015-3:1999 Methods of test for mortar for masonry Part 3: Determination of consistence of fresh mortar (by flow table)", European Committee for Standardization, Brussels, Belgium, 2000.

[32] Panda, B., Paul, S. C., Hui, L. J., Tay, Y. W. D., Tan, M. J. "Additive manufacturing of geopolymer for sustainable built environment", Journal of Cleaner Production, 167, pp. 281–288, 2017. https://doi.org/10.1016/j.jclepro.2017.08.165

[33] European Committee for Standardization "EN 12390-3:2019 Testing hardened concrete - Part 3: Compressive strength of test specimens", European Committee for Standardization, Brussels, Belgium, 2019.

[34] European Committee for Standardization "EN 12390-5:2019 Testing hardened concrete - Part 5: Flexural strength of test specimens", European Committee for Standardization, Brussels, Belgium, 2019.

[35] European Committee for Standardization "EN 12390-13:2013 Testing hardened concrete - Part 13: Determination of secant modulus of elasticity in compression", European Committee for Standardization, Brussels, Belgium, 2013.

[36] European Committee for Standardization "EN 1936:2006 Natural stone test methods - Determination of real density and apparent density, and of total and open porosity", European Committee for Standardization, Brussels, Belgium, 2007.

[37] Biró, A., Hlavička, V., Lublóy, É. "Effect of fire-related temperatures on natural stones", Construction and Building Materials, 212, pp. 92–101, 2019. https://doi.org/10.1016/j.conbuildmat.2019.03.333

[38] Roussel, N., Ovarlez, G., Garrault, S., Brumaud, C. "The origins of thixotropy of fresh cement pastes", Cement and Concrete Research, 42(1), pp. 148–157, 2012. https://doi.org/10.1016/j.cemconres.2011.09.004

[39] Panda, B., Singh, G. V. P. B., Unluer, C., Tan, M. J. "Synthesis and characterization of one-part geopolymers for extrusion based 3D concrete printing", Journal of Cleaner Production, 220, pp. 610–619, 2019.
https://doi.org/10.1016/j.jclepro.2019.02.185

[40] Chen, Y., Chaves Figueiredo, S., Li, Z., Chang, Z., Jansen, K., Çopuroğlu, O., Schlangen, E. "Improving printability of limestone-calcined clay-based cementitious materials by using viscosity-modifying admixture", Cement and Concrete Research, 132, 106040, 2020.
https://doi.org/10.1016/j.cemconres.2020.106040

[41] Le, T. T., Austin, S. A., Lim, S., Buswell, R. A., Law, R., Gibb, A. G. F., Thorpe, T. "Hardened properties of high-performance printing concrete", Cement and Concrete Research, 42(3), pp. 558–566, 2012.
https://doi.org/10.1016/j.cemconres.2011.12.003

[42] Wolfs, R. J. M., Bos, F. P., Salet, T. A. M. "Hardened properties of 3D printed concrete: The influence of process parameters on interlayer adhesion", Cement and Concrete Research, 119, pp. 132–140, 2019.
https://doi.org/10.1016/j.cemconres.2019.02.017

[43] Ma, G., Li, Z., Wang, L., Wang, F., Sanjayan, J. "Mechanical anisotropy of aligned fiber reinforced composite for extrusion-based 3D printing", Construction and Building Materials, 202, pp. 770–783, 2019.
https://doi.org/10.1016/j.conbuildmat.2019.01.008

[44] Pham, L., Tran, P., Sanjayan, J. "Steel fibres reinforced 3D printed concrete: Influence of fibre sizes on mechanical performance", Construction and Building Materials, 250, 118785, 2020.
https://doi.org/10.1016/j.conbuildmat.2020.118785